

# Short Papers

## Experimental Validation of a Feed-Forward Predictor for the Spring-Loaded Inverted Pendulum Template

Ismail Uyanık, Ömer Morgül, and Uluc Saranlı

**Abstract**—Widely accepted utility of simple spring–mass models for running behaviors as descriptive tools, as well as literal control targets, motivates accurate analytical approximations to their dynamics. Despite the availability of a number of such analytical predictors in the literature, their validation has mostly been done in simulation, and it is yet unclear how well they perform when applied to physical platforms. In this paper, we extend on one of the most recent approximations in the literature to ensure its accuracy and applicability to a physical monopodal platform. To this end, we present systematic experiments on a well-instrumented planar monopod robot, first to perform careful identification of system parameters and subsequently to assess predictor performance. Our results show that the approximate solutions to the spring-loaded inverted pendulum dynamics are capable of predicting physical robot position and velocity trajectories with average prediction errors of 2% and 7%, respectively. This predictive performance together with the simple analytic nature of the approximations shows their suitability as a basis for both state estimators and locomotion controllers.

**Index Terms**—Collision losses, legged locomotion, model verification, monopodal robots, parametric system identification, spring-loaded inverted pendulum (SLIP).

### I. INTRODUCTION

FACED with an ever-increasing need for mobile robotic platforms that can negotiate complex outdoor surfaces, it has become evident that traditional wheeled and tracked designs are approaching their morphological limits, and the use of legs in various forms has to be explored [1]. Recent research and progress in both the theory [2] and practice [3], [4] of building such machines provide ample evidence to support this observation. Nevertheless, numerous challenges remain before legged platforms can reach the level of autonomous performance already commonly observed in mobile robots.

The ultimate promise of nimble locomotion on complex terrain led to both the construction of many legged morphologies as well as mathematical models to describe their underlying dynamics. Among the latter, the spring-loaded inverted pendulum (SLIP) model [5], an extended version of which is illustrated

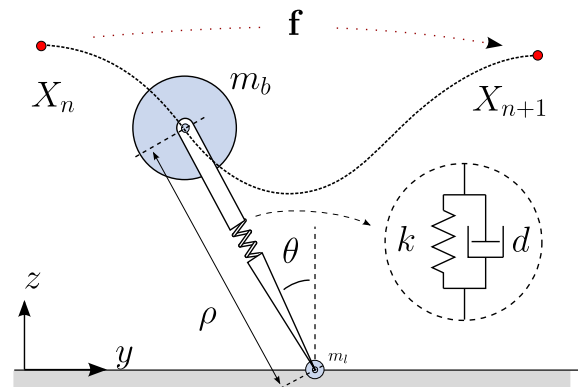


Fig. 1. Extended SLIP model. Dashed curve illustrates a single stride from one apex event to the next, defining the return map  $X_{n+1} = f(X_n, u_n)$ .

in Fig. 1, has become one of the most widely accepted and utilized, capable of accurately describing center-of-mass (COM) movements of running animals of widely varying sizes and morphologies [6], [7]. Originally motivated by biomechanical observations [8], [9], the SLIP model was adopted and refined by numerous robotics researchers over the past three decades [10], being established as an effective and appropriate dynamic abstraction for running behaviors [11].

The utility of this behavioral abstraction was also shown by its active embedding within more complex morphologies such as the RHex hexapod [12]. This provided further support to the idea pioneered by Raibert's robots [10] and other similar platforms [13]–[15] that the SLIP model could also act as the basis for hierarchical control strategies wherein the abstract running behavior would be regulated by SLIP controllers, unaware of the remaining redundancies in the complex morphology [16], [17].

The availability of analytic solutions to SLIP dynamics is crucial for formulating predictors for future steps as well as model-based controllers. Unfortunately, the nonintegrability of stance dynamics for the SLIP model necessitates approximate solutions, for which a number of alternatives have been proposed in the literature. In this context, Schwind and Koditschek proposed an iterative method that converges to the true SLIP dynamics under certain assumptions [18]. Subsequently, Geyer *et al.* formulated a simpler approximation based on certain assumptions on model parameters and trajectories [19]. Geyer's work was later extended with support for nonsymmetric steps [20] and viscous damping in the leg [21]. Note that the extended SLIP model that we use in this paper considers the viscous damping in the leg as well as the effects of nonsymmetric steps.

Manuscript received October 9, 2014; accepted December 15, 2014. Date of publication January 6, 2015; date of current version February 4, 2015. This paper was recommended for publication by Associate Editor P. Soueres and Editor T. Murphey upon evaluation of the reviewers' comments. This work was supported by the National Scientific and Technological Council of Turkey (TUBITAK) through Project 109E032. The work of I. Uyanık was supported by TUBITAK and Aselsan.

I. Uyanık and Ö. Morgül are with the Department of Electrical and Electronics Engineering, Bilkent University, 06800 Ankara, Turkey (e-mail: uyanik@ee.bilkent.edu.tr; morgul@ee.bilkent.edu.tr).

U. Saranlı is with the Department of Computer Engineering, Middle East Technical University, 06800 Ankara, Turkey (e-mail: saranli@ceng.metu.edu.tr).

Color versions of one or more of the figures in this paper are available online at <http://ieeexplore.ieee.org>.

Digital Object Identifier 10.1109/TRO.2014.2383531

Experimental evidence for the relevance of the SLIP model to both biological and robotic running behaviors has been established in a number of studies [12], [22]. However, the accuracy of approximate solutions to the dynamics of this model have so far only been verified in simulation [19], [21], leaving their practical applicability an open question. The validity of analytical predictors for SLIP trajectories strongly influences their usability in the design of model-based controllers [23]. The main goal of this paper is to establish that even approximate solutions to the SLIP model remain accurate for a physical platform. Similar to the work presented in this paper, Long *et al.* performed an experimental validation of approximate solutions to the simplest Parkour model (SPM) on ParkourBot [24], i.e., a planar dynamic climbing robot with two compliant legs, exhibiting SLIP-like behavior. Unlike SPM, which relies on an instantaneous stance phase, we consider the full stance dynamics as proposed in [21].

Our primary contribution in this paper is, hence, the experimental validation of a feed-forward predictor for SLIP dynamics. To this end, we also present the design of a well-instrumented monopod robot on which our validation experiments are performed. We also extend the solution presented in [21] to model the effects of nonnegligible leg mass on system energy, an inescapable aspect of every legged platform, and viscous damping during the flight phase that can be used to model unexpected sources of energy loss. As a final step, we compare the prediction performance of our predictor with Geyer's approximation [19] as well as the numeric integration of SLIP model with and without damping in the leg.

## II. EXTENDED SPRING-LOADED INVERTED PENDULUM MODEL

We begin our investigation by extending the ideal SLIP model to incorporate features necessary for its applicability to a physical monopod platform. First, we consider the effects of nonnegligible leg mass, which is an inevitable component of all legged platforms effecting system dynamics both due to its moment of inertia and collision losses. Previous studies in this context focused on the effect of leg mass on gait stability considering its effects both throughout the entire stride [25] as well as just the touchdown collision [26]. Our extended model incorporates the latter, focusing on the energetic effects of the leg mass due to phase transitions with collision, since swing leg dynamics were found to have only a minor effect on locomotory dynamics [25]. We will also show that the omission of leg dynamics during stance does not significantly impair the accuracy of our approximations for monopodal systems. The inclusion of this extension in our model substantially increases its applicability to physical legged platforms.

The second extension we consider is the presence of viscous damping during flight. Even though this is primarily useful to us for modeling mechanical properties of the central boom attachment for planarized robots such as our experimental platform, it generalizes the equations of motion in a way that allows modeling energy loss during flight for physical systems as well. This might be employed, for example, when leg retraction is found

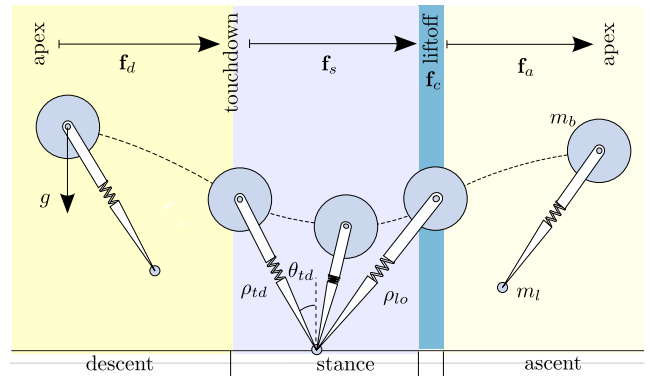


Fig. 2. SLIP locomotion phases (shaded regions) and transition events (boundaries).

to effect flight dynamics or when air friction is found to be significant for fast running.

It would certainly have been desirable to integrate lateral dynamics or a torso in our model. However, it has been shown that the dynamics of steady-state running in three dimensions is largely determined by motion occurring in the sagittal plane, with negligible influence from the lateral plane [10]. Moreover, to the best of our knowledge, there are currently no analytical approximations to the dynamics of a 3-D SLIP with a torso and the feasibility of obtaining such approximations is not yet clear. Consequently, even though this is a problem that deserves and requires further theoretical and experimental investigation, we leave this inquiry outside the scope of this paper.

Note that the extensions we consider do not alter the analytical simplicity of the SLIP predictor and preserve the generality of our results. Both of our extensions can be adapted to different monopodal robot platforms by calibrating the leg mass and viscous damping during flight, whatever its source might be. In addition, our model reduces to the ideal SLIP when the leg mass and flight damping are chosen to be zero, making our model applicable to a broad set of scenarios.

### A. Model Structure and Definitions

The extended SLIP model that we consider in this paper consists of a point mass attached to a compliant leg with mass  $m_l$  concentrated at the toe, stiffness  $k$ , and viscous damping  $d$  as illustrated in Fig. 1. During locomotion, this model alternates between *stance* and *flight* phases as shown in Fig. 2, with the toe remaining stationary on the ground during stance. No torque is applied to the leg during stance and the body experiences gravitational acceleration with both vertical and horizontal viscous damping during flight. Table I details the notation we use throughout the paper.

Touchdown and liftoff events mark transitions to and from the stance phase, respectively. Touchdown occurs when the toe comes into contact with the ground with the leg positioned at a fixed touchdown angle,  $\theta_{td}$ , during flight. We assume negligible toe dynamics during flight, with the toe mass positioned as necessary to achieve the desired touchdown leg angle and an uncompressed leg spring.

TABLE I  
NOTATION USED THROUGHOUT THE PAPER

Parameter	Description
$y, z, \dot{y}, \dot{z}$	Body positions and velocities
$m_b, m_l$	Body and leg mass of the robot
$k, d$	Leg spring and damping constants
$d_h, d_v$	Horizontal and vertical viscous damping during flight
$\rho, \theta$	Leg length and angle

Note that subscripts represent the system parameters at critical times such as  $\rho_{td}, \rho_b$ , and  $\rho_{lo}$  represent the leg length at touchdown, bottom, and liftoff times, respectively.

As usual, our study of this legged system relies on a Poincaré section defined at the ‘‘apex’’ point, defined as the highest point on system trajectories during flight with  $\dot{z} = 0$ .

This leads to the definition of apex states as

$$X_n := [y_n, \dot{y}_n, z_n]^T \quad (1)$$

which is subsequently used to define the apex return map

$$X_{n+1} = \mathbf{f}(X_n, \mathbf{u}) \quad (2)$$

with control inputs  $\mathbf{u}$  appropriately defined as in [21].

In contrast, liftoff occurs when the vertical component of the ground reaction force on the toe becomes negative. Unlike existing ideal SLIP models, our extended model incorporates a discrete change in the body velocity at liftoff due to the collision between the leg structure and a mechanical hard limit on the leg length, typically included on almost all prismatic leg designs to prevent radial leg oscillations during flight. We model this discontinuity with an instantaneous liftoff map. Consequently, the apex return map can be decomposed as

$$X_{n+1} := (\mathbf{f}_a \circ \mathbf{f}_c \circ \mathbf{f}_s \circ \mathbf{f}_d)(X_n, \mathbf{u}) \quad (3)$$

combining the descent map  $\mathbf{f}_d$ , the stance map  $\mathbf{f}_s$ , the instantaneous liftoff map  $\mathbf{f}_c$ , and the ascent map  $\mathbf{f}_a$ . Subsequent sections detail analytic derivations for each of these maps.

### B. Descent and Ascent Maps

In contrast with the simple ballistic flight trajectories of [21], flight dynamics for the extended model have viscous damping in both horizontal and vertical directions. The associated equations of motion take the form

$$\begin{bmatrix} \ddot{y} \\ \ddot{z} \end{bmatrix} = \begin{bmatrix} -d_h \dot{y} \\ -g - d_v \dot{z} \end{bmatrix} \quad (4)$$

where  $d_h$  and  $d_v$  correspond to horizontal and vertical viscous damping during flight, respectively.

Analytic solutions to these equations are given by

$$y(t) = \frac{\dot{y}_0}{d_h} (1 - e^{-d_h t}) + y_0 \quad (5)$$

$$z(t) = \frac{g}{d_v^2} (1 - e^{-d_v t} - d_v t) + \frac{\dot{z}_0}{d_v} (1 - e^{-d_v t}) + z_0 \quad (6)$$

where  $(y_0, z_0)$  and  $(\dot{y}_0, \dot{z}_0)$  represent initial body positions and velocities, respectively. Velocity equations for the body can be obtained through differentiation as

$$\dot{y}(t) = \dot{y}_0 e^{-d_h t} \quad (7)$$

TABLE II  
NOTATION FOR NONDIMENSIONAL PARAMETERS

Parameter	Definition	Description
$\bar{t}$	$:= t/\lambda$	Time (where $\lambda := \sqrt{\rho_0/g}$ )
$[\bar{\rho}, \bar{\theta}]$	$:= [\rho/\rho_0, \theta]$	Leg length and leg angle
$\kappa$	$:= k(\rho_0/(m_b g))$	Leg spring stiffness
$c$	$:= d(\rho_0/(\lambda m_b g))$	Leg viscous damping
$\bar{p}_\theta$	$:= p_\theta/(\lambda/(m_b \rho_0^2))$	Angular momentum

$$\dot{z}(t) = \dot{z}_0 e^{-d_v t} - \frac{g}{d_v} (1 - e^{-d_v t}). \quad (8)$$

Using these solutions, time of touchdown can be found as the solution to the equation  $z(t_{td}) = \rho \cos \theta_{td}$ , whereas time of apex is the solution to the equation  $\dot{z}(t_a) = 0$ .

### C. Approximate Analytical Solutions to Stance Trajectories

This section briefly summarizes the approximations we proposed in earlier work [21]. Using a nondimensional formulation, we redefine time as  $\bar{t} := t/\lambda$  with  $\lambda := \sqrt{\rho_0/g}$  and scale all distances with the spring rest length  $\rho_0$  to obtain equations of motion for stance in polar coordinates as

$$\ddot{\bar{\rho}} = \bar{\rho} \dot{\bar{\theta}}^2 - \kappa(\bar{\rho} - 1) - c\dot{\bar{\rho}} - \cos(\bar{\theta}) \quad (9)$$

$$0 = \frac{d}{d\bar{t}}(\bar{\rho}^2 \dot{\bar{\theta}}) - \bar{\rho} \sin \bar{\theta}. \quad (10)$$

Note that  $(d/d\bar{t})^n = \lambda^n (d/dt)^n$ , where all time derivatives are with respect to the newly defined scaled time variable. Table II details descriptions and definitions of nondimensional parameters used throughout the paper.

We now define for the natural frequency  $\hat{\omega}_0 := \sqrt{\kappa + 3\bar{p}_\theta^2}$ , the damping ratio  $\xi := c/(2\hat{\omega}_0)$ , the damped frequency  $\omega_d := \hat{\omega}_0 \sqrt{1 - \xi^2}$ , and the forcing term  $F := -1 + \kappa + 4\bar{p}_\theta^2$ . Assuming the conservation of angular momentum and following approximations introduced in [21], approximate analytical solutions to stance trajectories can be computed as

$$\bar{\rho}(\bar{t}) = M e^{-\xi \hat{\omega}_0 \bar{t}} \cos(\omega_d \bar{t} + \phi) + F/\hat{\omega}_0^2 \quad (11)$$

$$\dot{\bar{\rho}}(\bar{t}) = -M \hat{\omega}_0 e^{-\xi \hat{\omega}_0 \bar{t}} \cos(\omega_d \bar{t} + \phi + \phi_2) \quad (12)$$

$$\begin{aligned} \bar{\theta}(\bar{t}) = & \bar{\theta}_{td} + X \bar{t} + Y (e^{-\xi \hat{\omega}_0 \bar{t}} \cos(\omega_d \bar{t} + \phi - \phi_2) \\ & - \cos(\phi - \phi_2)) \end{aligned} \quad (13)$$

$$\dot{\bar{\theta}}(\bar{t}) = 3\bar{p}_\theta - 2\bar{p}_\theta F/\hat{\omega}_0^2 - 2\bar{p}_\theta M e^{-\xi \hat{\omega}_0 \bar{t}} \cos(\omega_d \bar{t} + \phi) \quad (14)$$

where  $M := \sqrt{A^2 + B^2}$ ,  $\phi := \arctan(-B/A)$ ,  $\phi_2 := \arctan(-\sqrt{1 - \xi^2}/\xi)$ ,  $A := \rho_{td} - F/\hat{\omega}_0^2$ , and  $B := (\dot{\rho}_{td} + \xi \hat{\omega}_0 A)/\omega_d$ .

This approximate solution for stance trajectories allows us to find the time of occurrence for bottom and liftoff transitions. Bottom is reached when the leg is maximally compressed and can be found as the solution to the equation  $\dot{\rho} = 0$ . The liftoff event is more challenging since the presence of damping often results in the toe lifting off the ground prior to the spring

reaching its rest length. Its time is computed as the minimum of these two conditions. Once these boundaries of the stance phase are found, the trajectories for an entire stride from an apex to the next can be computed. A final stage in [21] introduces a correction for the effect of gravity on the angular momentum during stance by adding a constant offset  $\bar{p}_{\bar{\theta}}(\bar{t}_{td})$  to the angular momentum at touchdown to increase the domain of validity for the approximations, preserving the analytical structure of the solution. This correction on the angular momentum is formulated as

$$\hat{p}_{\bar{\theta}} = \bar{p}_{\bar{\theta}}(\bar{t}_{td}) + \frac{\bar{t}_{lo}}{4} (\bar{\rho}(\bar{t}_{td}) \sin \bar{\theta}(\bar{t}_{td}) + \bar{\rho}(\bar{t}_{lo}) \sin \bar{\theta}(\bar{t}_{lo})) . \quad (15)$$

#### D. Modeling the Liftoff Collision

The liftoff event marks the end of stance. For the extended model, this is accompanied by an inelastic collision between the body and the leg structure, after which both masses end up moving with the same velocity. This is captured in our model as an instantaneous liftoff map (collision map)  $\mathbf{f}_c$ , corresponding to a discontinuity in the body velocity with

$$[\dot{y}^+, \dot{z}^+]^T := \frac{m_b}{m_b + m_l} [\dot{y}^-, \dot{z}^-]^T \quad (16)$$

where  $m_b$  and  $m_l$  are the body and leg masses, while the  $-$  and  $+$  superscripts identify precollision and postcollision states, respectively. Even though the toe may have lifted off the ground prior to this collision (hence resulting in nonzero toe velocity prior to collision), its effect on the body through leg damping will also contribute to the decrease in the body velocity. We represent the entirety of this “liftoff phase” with the inelastic collision of (16), which has approximately the same energetic effect on system velocities since no external forces except gravity act on the system after liftoff and the leg mass is assumed to be small.

With all the maps in place, we now have an analytical approximation to the return map defined in (2). Subsequent sections use this map for comparisons with experimental data collected for a wide range of initial conditions and parameters for the extended SLIP model.

### III. EXPERIMENTAL SETUP

Our focus in this paper is the experimental evaluation of the predictive performance of our analytical approximations to SLIP trajectories within a *single stride*. To this end, we have designed and constructed a monopodal platform based on the SLIP morphology, instrumented to provide state measurements while constraining robot motion to the sagittal plane. In this section, we first describe our experimental platform and, then, conduct systematic experiments to identify various dynamic parameters for our setup.

#### A. Robot Platform

Our platform consists of the planarizer illustrated in Fig. 3 that constrains the motion of an end-plate to a cylindrical plane, approximating unconstrained motion in the sagittal plane while eliminating unmodeled lateral dynamics. Such designs are commonly used to investigate locomotion systems and their

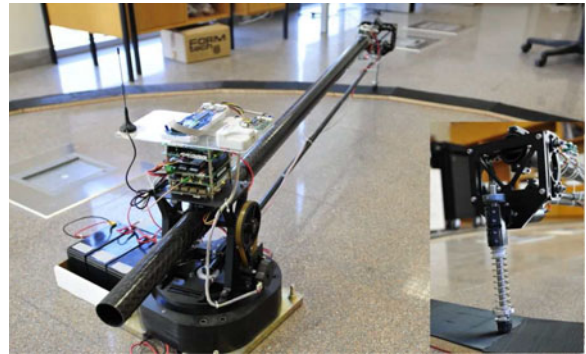


Fig. 3. Hopper robot with an overall view of the planarizer and close view of the leg.

correspondence to sagittal plane models [10], [14], [27], while allowing sustained forward locomotion.

An important feature of our design is its ability to provide accurate and high-bandwidth positional measurements through optical encoders mounted on the central joint assembly. The main boom, a 5-cm-diameter 1.67-m-long carbon-fiber tube, is connected to the central joint assembly, which has incremental encoders with 8192 counts per revolution connected to each axis through 1:6 timing belts. This yields a resolution of 0.21 mm in positional measurements.

The leg structure, also illustrated in Fig. 3, is affixed to the boom endplate, which is constrained to a fixed orientation in the sagittal plane. The rest length of the robot leg is 22 cm, and it is coupled to the boom plate through a DC motor, inactive during stance but used during flight to maintain a fixed leg angle prior to touchdown. The hip motor is a Maxon RE30-268215 60W brushed DC motor combined with a Maxon GP-32-C 1:18 planetary gear and is completely disabled during stance. A three-channel Type L MR encoder with 512 counts per revolution is used to measure the leg angle relative to the boom plate and, hence, the sagittal plane horizontal.

All computation is performed at the center of the planarizer with a Cool LiteRunner-LX800 PC104 single-board computer used for central control and the Universal Robot Bus architecture used for communication with peripheral units such as the motor amplifiers and encoder interfaces [28].

#### B. Data Collection and Preprocessing

The planarized monopod platform we described in preceding sections is used for all the experiments presented in this paper. To ensure general relevance of our results, we used four different helical springs, *hard*, *medium*, *soft*, and *softer*, manufactured to have the same rest length but different stiffnesses. The identified compliance and damping values for each of these springs can be seen in Table V. Note that the stiffness range was chosen to be consistent with biomechanics literature. In particular, experiments on humans (with 80-kg mass and 1-m leg length on average) running at different speeds (in the range 2.5–6.5 m/s) reveal leg stiffnesses in the range 12–42 kN/m [29], which corresponds to the stiffness range 15–53 in nondimensional coordinates. On the other hand, manual measurements of our leg springs yield a

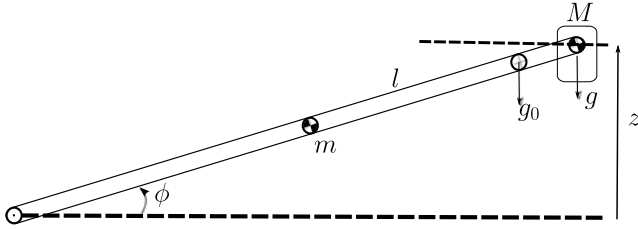


Fig. 4. Simplified lateral model for the boom and the leg assembly during flight.

stiffness range 16–43 in nondimensional units, which covers a large portion of the human stiffness range reported in [29].

Each experiment consisted of manually throwing the robot with different initial conditions, ensuring in each case that the vertical velocity was upwards to guarantee the occurrence of the first apex. Prior to this initial thrust, the leg was positioned at a desired angle (varied across different experiments), maintained throughout the initial flight phase using the hip motor without affecting flight dynamics. Upon touchdown, the hip motor was deactivated, letting natural SLIP stance dynamics govern the motion. Immediately following liftoff, the hip motor was reactivated to maintain the liftoff leg angle until the second apex point was reached, following which it was positioned vertically to catch the robot and stop its motion. An example for such an experiment is illustrated in Fig. 5, with the corresponding analytical solutions superimposed as dashed lines.

All system states were recorded during the experiment at 500 Hz using encoders mounted on the central assembly and the hip motor. Problematic experiments with foot slippage or other erroneous conditions were manually eliminated. Subsequently, positional data for clean experiments were filtered with a zero-phase fifth-order Butterworth filter with a cutoff frequency of 50 Hz to eliminate noise resulting from the oscillations and vibration of the boom. These positional encoder measurements were then numerically differentiated to obtain body velocity information. Following this filtering, key transition points along the trajectory, touchdown, bottom, liftoff, and apex were extracted based on their corresponding transition conditions and used for analysis and fitting.

### C. Modeling of the Boom Dynamics

The COM of the boom–leg assembly is situated outside the sagittal plane of locomotion. However, since the SLIP model is formulated in this sagittal plane, we capture the inertial effect of the boom as an increased gravitational acceleration on the robot body. A simplified lateral model of the boom assembly is shown in Fig. 4, with the equations of motion taking the form

$$(I + Ml^2) \ddot{\phi} = -Mlg_0 \cos \phi - 0.5mlg_0 \cos \phi \quad (17)$$

where  $m$  and  $I$  are the mass and moment of inertia for the boom, respectively, and  $M$  is the mass of the leg assembly. Assuming that  $\phi$  stays small with  $\cos \phi \approx 1$  and  $\sin \phi \approx \phi$ , we have

$$(I + Ml^2) \ddot{\phi} \approx -Mlg_0 - 0.5mlg_0. \quad (18)$$

Vertical robot position depends on the boom angle through  $z = l \sin \phi$ . For this relation, our small angle approximation

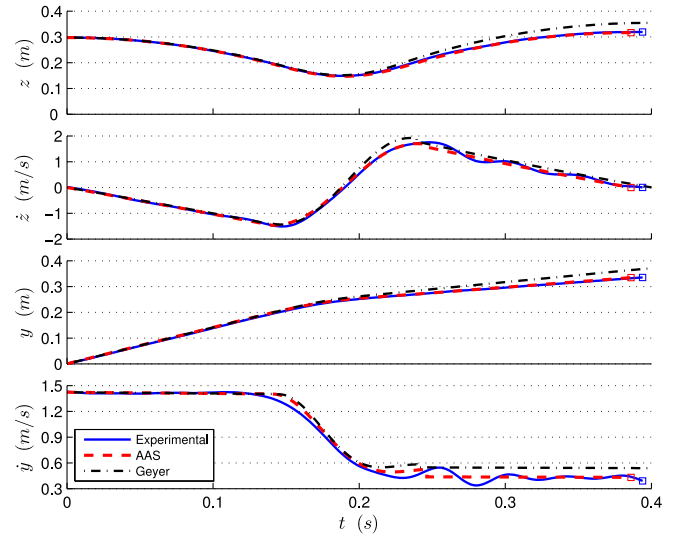


Fig. 5. Example stride for the hard spring with experimental data (solid blue) and analytic predictions of AAS (dashed red) and Geyer's method (dashed black) for position and velocity trajectories are shown together.

yields  $z \approx l\phi$ , whose second derivative  $\ddot{z} \approx l\ddot{\phi}$  can be combined with (18) to yield

$$\ddot{z} \approx \frac{M + m/2}{M + m/3} g_0 \quad (19)$$

where we used  $I = ml^2/3$  considering that the boom is a cylinder rotating around its tip. For our platform, we have  $M = 3.4$  kg and  $m = 0.39$  kg, which yields the gravitational acceleration perceived in the body frame as  $g = 9.99$  m/s<sup>2</sup>.

## IV. IDENTIFICATION OF THE EXPERIMENTAL PLATFORM

The two primary sources of inaccuracies in the predictive performance of our extended model are incorrect choices of model parameters and inherent deficiencies in the model or associated approximations. In this paper, we seek to isolate the latter to provide a fair assessment of our model and analytic approximations (AAS). Consequently, we use system identification methods to estimate dynamic model parameters, which are difficult to measure. Similar parameter identification methods have been used in the literature to determine accurate models for complex legged platforms [30], but our focus is on the validation of our approximations.

### A. Identification of Body and Leg Masses

We first focus our system identification efforts on the body and leg mass parameters,  $m_b$  and  $m_l$  respectively, for the extended SLIP model since their influence on system dynamics, particularly energy losses due to the liftoff collision are substantial. To this end, we first use vertical hopping experiments with the leg kept vertical by the hip motor. For the flight phase, (6) and (8) remain valid and yield the vertical position and velocity. In contrast, stance trajectories (11)–(14) take a much simpler form when we constrain the motion to vertical dimension.

Using the data collection and filtering procedure described in Section III-B, we ran 50 vertical experiments for each one

TABLE III  
ESTIMATES OF MASS AND VERTICAL DAMPING PARAMETERS  
BASED ON VERTICAL EXPERIMENTS

$m_b$ (kg)	$m_l$ (kg)	$d_v$ (N·s/m)
3.21	0.19	0.06

of all four springs for a total of 200 experiments with  $\theta_{td} = 0$  and  $\dot{y}_0 = 0$ . Analytic solutions for these vertical trajectories have three common parameters: the body mass  $m_b$ , the leg mass  $m_l$ , and the vertical flight damping  $d_v$  in addition to the spring specific compliance  $k$  and damping  $d$  parameters. In order to find these parameters, we construct a nonlinear least-squares problem with the cost function defined as the percentage difference between measured and predicted apex and bottom positions, taking the form

$$C_v := \frac{\| [z_a, z_b] - [\hat{z}_a, \hat{z}_b] \|_2}{\| [z_a, z_b] \|_2}. \quad (20)$$

We use MATLAB's `lsqnonlin` function to find solutions for  $m_b$ ,  $m_l$ , and  $d_v$  common to all 200 experiments. Our results are shown in Table III, while stiffness and damping parameters for all four springs are detailed in Table V.

#### B. Identification of Horizontal Flight Damping

Vertically constrained experiments do not exercise horizontal degrees of freedom in our boom assembly. Consequently, we use our entire set of single-stride experiments to identify the horizontal damping coefficient during flight.

We begin by introducing a first-order approximation to horizontal flight dynamics, which normally have exponential decay terms in their solution, making linear fitting methods inapplicable. In particular, we will assume that the horizontal velocity during the descent phase can be approximated as

$$\dot{y}(t) \approx \dot{y}_0 - d_h t \quad (21)$$

while relaxing the initial condition  $\dot{y}_0$  to possibly be different than the measured initial condition  $\dot{y}(0)$  to increase the accuracy of the approximation. Recall that the parameter of interest in this fitting procedure is the damping coefficient  $d_h$ , which justifies this relaxation in the fitting.

Having identified touchdown states through the preprocessing steps described in Section III-B, we can now formulate a linear set of equations  $Ax = b$ , by equating multiple predicted and measured state points along each trajectory as

$$\begin{bmatrix} 1 & 0 & \cdots & 0 & t_1^1 \\ \vdots & & & & \vdots \\ 1 & 0 & \cdots & 0 & t_{n_1}^1 \\ \vdots & & & & \vdots \\ 0 & 0 & \cdots & 1 & t_1^m \\ \vdots & & & & \vdots \\ 0 & 0 & \cdots & 1 & t_{n_m}^m \end{bmatrix} \begin{bmatrix} \dot{y}_0^1 \\ \dot{y}_0^2 \\ \vdots \\ \dot{y}_0^m \\ -d_h \end{bmatrix} = \begin{bmatrix} \dot{y}^1(t_1^1) \\ \vdots \\ \dot{y}^1(t_{n_1}^1) \\ \vdots \\ \dot{y}^m(t_1^m) \\ \vdots \\ \dot{y}^m(t_{n_m}^m) \end{bmatrix} \quad (22)$$

where  $t_i^j$  is the  $i$ th data point for the  $j$ th experiment, with the corresponding horizontal velocity  $\dot{y}^j(t_i^j)$ . The best fit to this set of data points is given by the regressor

$$x = (A^T A)^{-1} A^T b. \quad (23)$$

Using this procedure, our experiments result in the horizontal flight damping coefficient common to all experiments identified as  $d_h = 0.3$  N·s/m.

#### V. EXPERIMENTAL VALIDATION OF ANALYTIC SOLUTIONS

Having identified fixed mass and flight damping parameters for the leg assembly and the planarizing boom, we now continue with the evaluation of the predictive performance of our AAS to the extended SLIP model together with the identification of spring compliance and damping coefficients for four different springs. In order to ensure the validity of our evaluation, we ran experiments with a wide range of initial conditions and touchdown leg angles as described in Section III-B. In particular, 181, 208, 267, and 174 valid experiments were completed for the softer, soft, medium, and hard springs, respectively, for a total of 830 experiments. The initial conditions for single stride experiments were chosen in the ranges  $\dot{y} \in [0.3, 2.5](\text{m/s})$  and  $z \in [0.24, 0.48](\text{m})$ .

#### A. Performance Criteria

As a common basis for our cost function for system identification as well as the evaluation of the predictive performance for our approximations, we first define apex position, velocity, and time error measures for each stride as

$$E_{ap} := 100 \frac{\| [y_a, z_a] - [\hat{y}_a, \hat{z}_a] \|_2}{\| [y_a, z_a] \|_2} \quad (24)$$

$$E_{av} := 100 \frac{\| \dot{y}_a - \hat{\dot{y}}_a \|_2}{\| \dot{y}_a \|_2} \quad (25)$$

$$E_{at} := 100 \frac{\| t_a - \hat{t}_a \|_2}{\| t_a \|_2} \quad (26)$$

where variables with hats denote our predictions. These definitions mirror similar measures defined in [21]. In order to improve convergence for the system identification, we also define a position error for the bottom transition as

$$E_{bp} := 100 \frac{\| [y_b, z_b] - [\hat{y}_b, \hat{z}_b] \|_2}{\| [y_b, z_b] \|_2}. \quad (27)$$

The cost function that we define for system identification is composed of four components corresponding to the error measures defined above, taking the form

$$C := \sqrt{C_{ap}^2 + C_{av}^2 + C_{at}^2 + C_{bp}^2} \quad (28)$$

where individual cost functions  $C_{ap}$ ,  $C_{av}$ ,  $C_{at}$ , and  $C_{bp}$  correspond to arithmetic mean of corresponding errors.

#### B. Predictive Performance With Cross Validation

In this section, we present a comprehensive evaluation of the predictive performance of our AAS to the extended SLIP

TABLE IV  
PERCENTAGE PREDICTION ERRORS AND PARAMETER ESTIMATES RESULTING FROM 30-FOLD CROSS-VALIDATION EXPERIMENTS

Method	Test Runs			Training Runs			Leg Parameters		
	$E_{ap}$	$E_{av}$	$E_{at}$	$E_{ap}$	$E_{av}$	$E_{at}$	$k$ (N/m)	$d$ (N-s/m)	
<b>Hard</b>	SLIPD	$1.41 \pm 0.51$	$3.98 \pm 1.04$	$1.69 \pm 0.62$	$1.36 \pm 0.01$	$3.75 \pm 0.04$	$1.54 \pm 0.02$	$6560 \pm 3.09$	$12.3 \pm 0.07$
	AAS	<b><math>1.53 \pm 0.40</math></b>	<b><math>4.23 \pm 1.12</math></b>	<b><math>1.74 \pm 0.54</math></b>	$1.52 \pm 0.02$	$4.21 \pm 0.04$	$1.74 \pm 0.02$	$6605 \pm 6.14$	$12.1 \pm 0.06$
	SLIP	$8.13 \pm 0.63$	$4.32 \pm 1.22$	$3.17 \pm 0.67$	$7.9 \pm 0.01$	$4.18 \pm 0.04$	$3.06 \pm 0.03$	$8136 \pm 9.06$	–
	Geyer	$10.46 \pm 0.43$	$8.82 \pm 2.28$	$2.74 \pm 0.99$	$10.45 \pm 0.03$	$8.68 \pm 0.07$	$2.75 \pm 0.04$	$11569 \pm 93.97$	–
<b>Medium</b>	SLIPD	$1.69 \pm 0.46$	$5.41 \pm 1.34$	$1.24 \pm 0.42$	$1.54 \pm 0.02$	$5.26 \pm 0.06$	$1.19 \pm 0.02$	$4931 \pm 7.00$	$11.3 \pm 0.05$
	AAS	<b><math>1.89 \pm 0.40</math></b>	<b><math>6.31 \pm 1.20</math></b>	<b><math>1.27 \pm 0.35</math></b>	$1.88 \pm 0.02$	$6.29 \pm 0.04$	$1.26 \pm 0.01$	$4828 \pm 6.83$	$11.9 \pm 0.05$
	SLIP	$7.43 \pm 0.56$	$6.24 \pm 1.35$	$3.44 \pm 0.32$	$6.92 \pm 0.01$	$5.34 \pm 0.06$	$3.47 \pm 0.04$	$5921 \pm 9.47$	–
	Geyer	$9.49 \pm 0.35$	$9.11 \pm 2.54$	$2.09 \pm 0.43$	$9.49 \pm 0.01$	$9.05 \pm 0.09$	$2.10 \pm 0.02$	$8308 \pm 30.50$	–
<b>Soft</b>	SLIPD	$1.88 \pm 0.72$	$5.56 \pm 2.34$	$1.98 \pm 0.64$	$1.83 \pm 0.02$	$5.34 \pm 0.06$	$1.72 \pm 0.02$	$3570 \pm 3.88$	$9.94 \pm 0.05$
	AAS	<b><math>2.07 \pm 0.66</math></b>	<b><math>7.54 \pm 2.45</math></b>	<b><math>2.68 \pm 0.72</math></b>	$2.06 \pm 0.02$	$7.54 \pm 0.08$	$2.68 \pm 0.03$	$3529 \pm 3.05$	$9.84 \pm 0.04$
	SLIP	$8.37 \pm 0.92$	$8.12 \pm 2.55$	$2.48 \pm 0.41$	$7.93 \pm 0.02$	$7.73 \pm 0.06$	$2.13 \pm 0.02$	$4645 \pm 2.34$	–
	Geyer	$12.29 \pm 0.68$	$15.25 \pm 4.12$	$3.47 \pm 0.91$	$12.28 \pm 0.03$	$15.23 \pm 0.13$	$3.48 \pm 0.04$	$7602 \pm 25.65$	–
<b>Softer</b>	SLIPD	$2.03 \pm 0.40$	$8.23 \pm 1.74$	$1.67 \pm 0.62$	$2.02 \pm 0.02$	$8.22 \pm 0.09$	$1.65 \pm 0.02$	$2598 \pm 5.79$	$5.33 \pm 0.05$
	AAS	<b><math>2.21 \pm 0.47</math></b>	<b><math>7.80 \pm 1.84</math></b>	<b><math>1.68 \pm 0.49</math></b>	$2.19 \pm 0.03$	$7.74 \pm 0.06$	$1.67 \pm 0.02$	$2572 \pm 4.18$	$6.49 \pm 0.03$
	SLIP	$7.14 \pm 0.86$	$11.57 \pm 2.36$	$3.06 \pm 0.61$	$5.95 \pm 0.01$	$9.19 \pm 0.11$	$2.79 \pm 0.03$	$3128 \pm 8.67$	–
	Geyer	$9.49 \pm 1.15$	$19.97 \pm 5.85$	$1.37 \pm 0.40$	$9.47 \pm 0.06$	$19.78 \pm 0.19$	$1.38 \pm 0.02$	$4117 \pm 29.88$	–

TABLE V  
ESTIMATED LEG COMPLIANCE AND DAMPING PARAMETERS

Spring:	Softer		Soft		Medium		Hard	
	$k$	$d$	$k$	$d$	$k$	$d$	$k$	$d$
SLIPD	2598	5.3	3570	9.9	4931	11.3	6560	12.3
AAS	<b>2572</b>	<b>6.5</b>	<b>3529</b>	<b>9.8</b>	<b>4828</b>	<b>11.9</b>	<b>6605</b>	<b>12.1</b>
SLIP	3128	–	4645	–	5921	–	8136	–
Geyer	4117	–	7602	–	8308	–	11569	–
Vertical	2600	6.7	3536	9.9	4972	12.4	6630	12.7
Manual	2322	–	2915	–	4298	–	6282	–

model, first identifying the stiffness and damping coefficients for the compliant leg, then using the error measures defined in Section V-A to quantify the accuracy of the approximations. In addition to AAS, we also evaluate the prediction performance of Geyer’s approximation [19] as well as the numeric integration of the original stance dynamics in (9) and (10) both with (SLIPD) and without (SLIP) viscous damping in the leg.

For statistical validity, we used a cross-validation approach by dividing experiments into disjoint subsets for training (estimating leg compliance and damping) and testing (evaluating predictive performance). In this context, we considered 5-fold, 10-fold, 30-fold and leave-one-out options and observed their results separately. Consistent with observations described in [31], we confirmed that using higher number of folds yields low deviations in training results but high deviations in test results. Consequently, we use 30-fold cross validation for this study, ensuring that test results represent the worst-case performance figures for our approximations.

For the estimation of leg compliance and damping from training data, we use the `lsqnonlin` method of MATLAB, which uses the *trust-region-reflective* optimization algorithm [32]. We use the compliance and damping parameters in Table V obtained from vertical experiments to initialize the optimization, further refining resulting parameters through repeated runs of the optimization.

Fig. 5 illustrates the results of our system identification for one of the experiments, showing filtered system states superimposed with the predictions of our AAS and Geyer’s predictor. Initial conditions for the analytic solutions were chosen to be the same as the experiment, except the initial horizontal velocity which uses the estimate obtained from (23). Velocity oscillations in the experimental data right after  $t = 0.235$  s are due to vibrations of the boom assembly following the liftoff collision (also visible as a discontinuity in horizontal and vertical velocities at around  $t = 0.235$  s), but dissipate long before the end of the stride and, hence, do not affect the predictive performance of the return map. Apart from this unmodeled effect, the extended SLIP model and our approximations show an accurate performance in capturing the behavior of the experimental platform as compared with Geyer’s predictor.

Table IV details average percentage prediction errors for apex position, velocity, and time as well as parameter estimations and their standard deviations across all experiments including training as well as test sets. Overall, our results show that prediction errors in positional, velocity, and time variables are 2%, 7%, and 1.85% on average, respectively. The standard deviations are also well below 0.1% and 2.5% for training and test data, respectively, as a result of 30-fold cross validation. Nevertheless, these experimentally validated single-stride prediction errors are sufficiently low to be compensated by using adaptive controllers such as in [23] when additional feedback can be introduced. Similarly, reactive control algorithms, which are robust against model and measurement uncertainty, can be used to compensate for such errors [33].

In contrast, numeric integration of the SLIP model and Geyer’s prediction show prediction errors around 10% on average for positional variables. The main reason for this significant error is the unmodeled but inescapable damping loss in experimental robot platforms. Note that AAS and Geyer’s predictor are approximations to SLIPD and SLIP dynamics, respectively. This is why numeric integrations perform better than their corresponding analytic predictors. Consequently, since the numeric

SLIP predictor represents an upper bound for the accuracy of all methods that approximate the trajectories of lossless SLIP models and still performs worse than our method, we have not included results from any other approximations in our comparative study.

We can also observe that prediction errors of AAS decrease with increasing spring stiffness, which is expected since stiffer springs compress less, with trajectories coming closer to satisfying the assumptions underlying our approximations [21]. In the case of hard spring, the average percentage position prediction error is 1.53%, which corresponds to approximately 0.75 cm for our robot running at a maximum height of 50 cm.

It is interesting to note that average prediction errors for AAS with respect to SLIPD were 0.75% and 1.40% for position and velocity coordinates, respectively [21]. However, the relative prediction performance of AAS with respect to SLIPD has drastically decreased to 0.1% on average in our experimental study. This is due to our fitting procedure, which allows AAS and SLIPD to choose different leg compliance and damping parameters in order to minimize their prediction errors.

Our system identification process also reveals leg compliance and damping parameters for all four springs. Due to our adoption of the 30-fold cross-validation approach, we obtain 30 different values for these parameters, whose mean and standard deviation figures are summarized in Table IV. Note that the estimated leg compliance and damping parameters through AAS and SLIPD are very close to those revealed by vertical experiments. On the contrary, estimation through Geyer's predictor and SLIP results in unrealistic leg compliance values, since they assume zero damping in the leg.

Finally, we have also investigated the dependence of prediction performance on the asymmetry of the stride trajectory with respect to the gravitational vector. The concept of a *neutral touchdown angle* plays an important role in the characterization of equilibrium gaits for the ideal SLIP model [5]. Moreover, AAS to SLIP trajectories preceding our contributions relied on the assumption of symmetric gaits, decreasing their efficacy for transient asymmetric steps. Consequently, an evaluation of how prediction performance degrades as the touchdown leg angle deviates from its neutral choice was investigated in [21], revealing that the gravity correction featured in approximations substantially improves prediction performance. We present a similar evaluation on our experimental platform in the remainder of this section.

We begin by defining the *relative angle*  $\theta_{td,rel}$  as

$$\theta_{td,rel} := \theta_{td} - \theta_{td,n} \quad (29)$$

to represent the deviation from the neutral angle  $\theta_{td,n}$ . An important difference from the corresponding definition in [21] is the fact that stance trajectories are never symmetric for our lossy SLIP model or the experimental platform. Consequently, our definition of a neutral angle focuses on forward velocity as the solution to the equation

$$\theta_{td,n} = \underset{\theta}{\operatorname{argmin}}((\dot{y}_n - \dot{y}_{n+1}(\theta))^2) \quad (30)$$

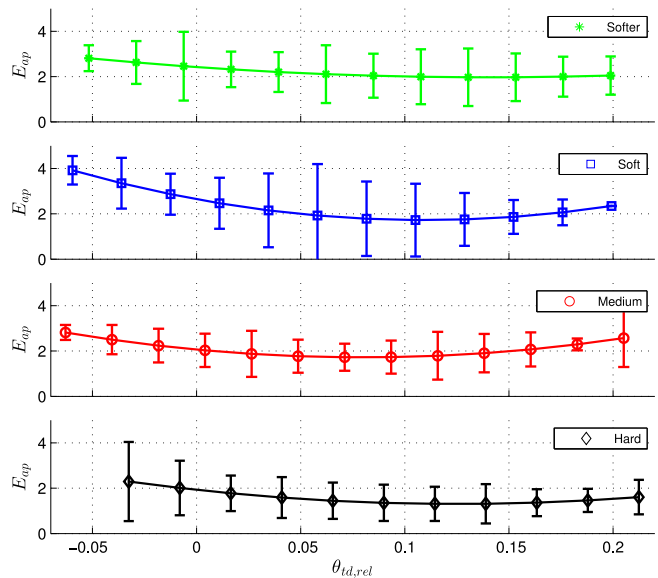


Fig. 6. Dependence of mean prediction errors in apex position to the deviation from the neutral touchdown angle (relative angle) for all leg springs.

which we use to compute the relative angle value corresponding to the initial condition associated with each experiment.

Fig. 6 shows our results for each of the four different spring stiffnesses, where marked data points represent different bins for the relative angle, and the vertical axes represent mean and standard deviation values for the average positional prediction errors all experiments grouped in each bin. Continuous graphs show quadratic fits to the mean errors in each bin to reveal the dependence of the errors on the relative angle and coincide very well with mean data. Our results are consistent with those obtained from pure simulation studies, confirming that the gravity correction introduced by our approximations substantially improves the degradation in prediction performance away from symmetric gaits with positional errors remaining below 5% even when considerable asymmetry is present in the stride.

## VI. CONCLUSION AND FUTURE WORK

In this paper, we have presented the experimental validation of an approximate but accurate feed-forward predictor we recently introduced for the well-known SLIP template. Our verification method first identifies unknown system parameters for our SLIP-based experimental platform and, then, evaluates prediction performance of the proposed predictor on the experimental data. We also compare the prediction performance of our predictor with Geyer's approximation as well as the numeric integration of SLIP dynamics with and without damping in the leg. Key extensions to the basic SLIP model, including viscous damping during flight and leg collision at liftoff, were also introduced to improve model performance in comparison with the experimental platform.

Our validation experiments include systematic tests by using four different leg springs, covering a large range of initial conditions and control inputs to show that the proposed map can provide accurate estimates for all trajectories of the experimental



platform. Our method not only provides an experimental validation strategy for the SLIP predictors but reveals insight into the effects of mechanical parameters of the physical robot platform as well. In particular, we observed that harder springs yield better prediction performance, confirming theoretical observations based on the nature of our approximations. Overall, our approximations can predict positional and velocity trajectories with mean 2% and 7%, respectively, well within the range of errors that can be tolerated by adaptive [23] or reactive [33] control strategies.

In addition to this performance characterization, we have also validated that the gravity correction incorporated by our approximations performs as predicted by investigating performance with respect to the relative touchdown angle, defined as the deviation from the touchdown angle that would yield symmetric locomotion. Our approximations preserve their accuracy even for nonsymmetric trajectories where the angular momentum around the toe is no longer conserved.

Our longer term goal is to design accurate model-based control algorithms and state estimation techniques for legged robot platforms. The applicability of such control algorithms would be substantially improved with more accurate predictions of associated single-stride trajectories. In the near future, we will implement and validate deadbeat control strategies based on our predictor, supported by adaptive algorithms based on the same predictor for online estimation of dynamic parameters. In the long term, we believe that accurate and efficient models of legged platforms will be instrumental in both understanding underlying principles of legged locomotion, as well as providing the necessary tools for high-performance controllers, estimators, and motion planners.

#### ACKNOWLEDGMENT

The authors would like to thank B. Yücesoy, H. E. Orhon, E. Kuzucu, M. Aslan, and B. Çatalbaş for their support during data collection.

#### REFERENCES

- [1] M. LaBarbera, "Why the wheels won't go," *Am. Naturalist*, vol. 121, no. 3, pp. 395–408, Mar. 1983.
- [2] P. Holmes, R. Full, D. Koditschek, and J. Guckenheimer, "The dynamics of legged locomotion: Models, analyses, and challenges," *SIAM Rev.*, vol. 48, no. 2, pp. 207–304, Feb. 2006.
- [3] U. Saranli, M. Buehler, and D. E. Koditschek, "RHEx: A simple and highly mobile robot," *Int. J. Robot. Res.*, vol. 20, no. 7, pp. 616–631, Jul. 2001.
- [4] D. Wooden, M. Malchano, K. Blankespoor, A. Howardy, A. A. Rizzi, and M. Raibert, "Autonomous navigation for BigDog," in *Proc. IEEE Int. Conf. Robot. Autom.*, 2010, pp. 4736–4741.
- [5] W. J. Schwind, "Spring loaded inverted pendulum running: A plant model," Ph.D. dissertation, Dept. Elect. Eng.: Systems, Univ. Michigan, Ann Arbor, MI, USA, 1998.
- [6] R. Blickhan and R. J. Full, "Similarity in multilegged locomotion: Bouncing like a monopode," *J. Comparative Physiol. A, Neuroethol., Sensory, Neural, Behavioral Physiol.*, vol. 173, no. 5, pp. 509–517, Nov. 1993.
- [7] C. T. Farley and D. P. Ferris, "Biomechanics of walking and running: Center of mass movements to muscle action," *Exercise Sport Sci. Rev.*, vol. 26, pp. 253–283, Jan. 1998.
- [8] R. M. Alexander, "Three uses for springs in legged locomotion," *Int. J. Robot. Res.*, vol. 9, no. 2, pp. 53–61, Apr. 1990.
- [9] R. M. Alexander and A. S. Jayes, "Vertical movement in walking and running," *J. Zoology*, vol. 185, no. 1, pp. 27–40, May 1978.
- [10] M. H. Raibert, *Legged Robots That Balance*. Cambridge, MA, USA: MIT Press, 1986.
- [11] R. J. Full and D. E. Koditschek, "Templates and anchors: Neuromechanical hypotheses of legged locomotion," *J. Exp. Biol.*, vol. 202, pp. 3325–3332, Dec. 1999.
- [12] R. Altendorfer, U. Saranli, H. Komsuoglu, D. E. Koditschek, H. Brown, M. Buehler, N. Moore, D. McMordie, and R. Full, "Evidence for spring loaded inverted pendulum running in a hexapod robot," in *Experimental Robotics VII* (Lecture Notes in Control and Information Sciences Series), vol. 271. Berlin, Germany: Springer, 2001, pp. 291–302.
- [13] P. Gregorio, M. Ahmadi, and M. Buehler, "Design, control, and energetics of an electrically actuated legged robot," *IEEE Trans. Syst., Man, Cybern. B, Cybern.*, vol. 27, no. 4, pp. 626–634, Aug. 1997.
- [14] G. Zeglin, "The bow leg hopping robot," Ph.D. dissertation, The Robotics Institute, Carnegie Mellon Univ., Pittsburgh, PA, USA, Oct. 1999.
- [15] J. W. Hurst, J. Chestnutt, and A. Rizzi, "Design and philosophy of the BiMASC, a highly dynamic biped," in *Proc. IEEE Int. Conf. Robot. Autom.*, 2007, pp. 1863–1868.
- [16] U. Saranli and D. E. Koditschek, "Template based control of hexapedal running," in *Proc. IEEE Int. Conf. Robot. Autom.*, 2003, pp. 1374–1379.
- [17] M. M. Ankarali and U. Saranli, "Control of underactuated planar pronking through an embedded spring-mass hopper template," *Auton. Robots*, vol. 30, no. 2, pp. 217–231, 2011.
- [18] W. J. Schwind and D. E. Koditschek, "Approximating the stance map of a 2 dof monopod runner," *J. Nonlinear Sci.*, vol. 10, no. 5, pp. 533–588, Jul. 2000.
- [19] H. Geyer, A. Seyfarth, and R. Blickhan, "Spring-mass running: Simple approximate solution and application to gait stability," *J. Theoretical Biol.*, vol. 232, no. 3, pp. 315–328, Feb. 2005.
- [20] O. Arslan, U. Saranli, and Ö. Morgül, "An approximate stance map of the spring-mass hopper with gravity correction for nonsymmetric locomotions," in *Proc. IEEE Int. Conf. Robot. Autom.*, 2009, pp. 2388–2393.
- [21] U. Saranli, O. Arslan, M. M. Ankarali, and Ö. Morgül, "Approximate analytic solutions to non-symmetric stance trajectories of the passive spring-loaded inverted pendulum with damping," *Nonlinear Dyn.*, vol. 62, pp. 729–742, Dec. 2010.
- [22] S. W. Lipfert, M. Gunther, D. Renjewski, S. Grimmer, and A. Seyfarth, "A model-experiment comparison of system dynamics for human walking and running," *J. Theoretical Biol.*, vol. 292, no. 0, pp. 11–17, 2012.
- [23] I. Uyanik, U. Saranli, and Ö. Morgül, "Adaptive control of a spring-mass hopper," in *Proc. IEEE Int. Conf. Robot. Autom.*, 2011, pp. 2138–2143.
- [24] A. Long, R. Gregg, and K. Lynch, "The simplest Parkour model: Modeling, experimental validation and stability analysis," presented at the *Int. Conf. Climbing Walking Robots*, Paris, France, 2011.
- [25] F. Peuker, A. Seyfarth, and S. Grimmer, "Inheritance of slip running stability to a single-legged and bipedal model with leg mass and damping," in *Proc. IEEE Int. Conf. Biomed. Robot. Biomechatronics*, 2012, pp. 395–400.
- [26] M. Hutter, C. D. Remy, M. A. Hopfinger, and R. Siegwart, "Slip running with an articulated robotic leg," in *Proc. IEEE/RSJ Int. Conf. Intell. Robots Syst.*, 2010, pp. 4934–4939.
- [27] A. Sato and M. Buehler, "A planar hopping robot with one actuator: Design, simulation, and experimental results," in *Proc. IEEE/RSJ Int. Conf. Intell. Robots Syst.*, 2004, vol. 4, pp. 3540–3545.
- [28] U. Saranli, A. Avci, and M. Ozturk, "A modular real-time fieldbus architecture for mobile robotic platforms," *IEEE Trans. Instrum. Meas.*, vol. 60, no. 3, pp. 916–927, Mar. 2011.
- [29] A. Arampatzis, G. P. Briggemann, and V. Metzler, "The effect of speed on leg stiffness and joint kinematics in human running," *J. Biomechanics*, vol. 32, pp. 1349–1353, 1999.
- [30] H. W. Park, K. Sreenath, J. Hurst, and J. W. Grizzle, "Identification of a bipedal robot with a compliant drivetrain: Parameter estimation for control design," *IEEE Control Syst. Mag.*, vol. 31, no. 2, pp. 63–88, Apr. 2011.
- [31] T. Hastie, R. Tibshirani, and J. Friedman, *The Elements of Statistical Learning: Data Mining, Inference, and Prediction*. Heidelberg, Germany: Springer-Verlag, 2001.
- [32] T. Coleman and Y. Li, "An interior trust region approach for nonlinear minimization subject to bounds," *SIAM J. Optim.*, vol. 6, no. 2, pp. 418–445, May. 1996.
- [33] O. Arslan and U. Saranli, "Reactive planning and control of planar spring-mass running on rough terrain," *IEEE Trans. Robot.*, vol. 28, no. 3, pp. 567–579, Jun. 2012.